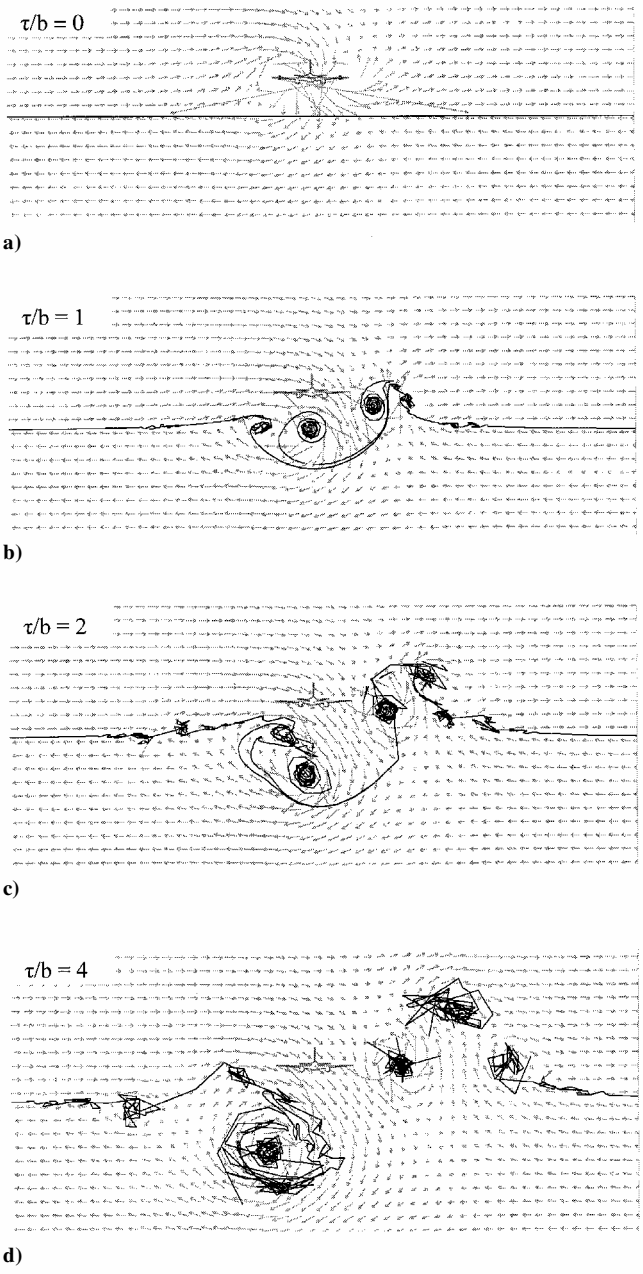

Fig. 2 Interaction of vortex pair and crosswind shear, initialized by Eqs. (2) and (3).

active turbulence, which tends to destabilize the vortex pair. On the other hand, convection is known to be the dominant factor in early stages of the vortex development, and flow patterns similar to those shown here have been found repeatedly, more recently in modeling the interactions with thick shear layers.[9]

Conclusions

Based on the convection of thin vortex sheets, it has been shown that aircraft vortices can temporarily intensify in the presence of crosswind shear. An aircraft following another one may, thus, be subjected to a stronger vortex than that expected in the wake of the leading aircraft in a quiescent atmosphere.

Although wake turbulence measurements may soon become a part of the aircraft airworthiness process, it is believed that still greater safety of air travel is achievable by minimizing the vortex intensification in wind shear and by avoiding wake vortex encounters as much as possible. This may involve guiding the aircraft to turn into crosswind only when sufficiently distant from the airports and equipping them, individually, with wind shear detectors, wake vortex sensors, and other suitable warning devices.

References

[1]Simpson, R. W., and Ausrotas, R., "A Critical Review of the FAA Safety Rulemaking on Wake Turbulence," Air Transport Association of America, Sept. 1997.

[2]Spalart, P. R., "Airplane Trailing Vortices," *Annual Review of Fluid Mechanics*, Vol. 30, 1998, pp. 107–138.

[3]Sarpkaya, T., "Decay of Wake Vortices of Large Aircraft," *AIAA Journal*, Vol. 36, No. 9, 1998, pp. 1671–1679.

[4]Chorin, A. J., *Vorticity and Turbulence*, Springer-Verlag, New York, 1994, pp. 84–89.

[5]Mokry, M., "Numerical Simulation of Aircraft Trailing Vortices Interacting with Ambient Shear or Ground," *Journal of Aircraft*, Vol. 38, No. 4, 2001, pp. 636–643.

[6]Schecter, D. A., and Dubin, D. H. E., "Theory and Simulations of Two-Dimensional Vortex Motion Driven by a Background Vorticity Gradient," *Physics of Fluids*, Vol. 13, No. 6, 2001, pp. 1704–1723.

[7]Proctor, F. H., "The NASA-Langley Wake Vortex Modelling Effort in Support of an Operational Aircraft Spacing," AIAA Paper 98-0589, Jan. 1998.

[8]Zheng, Z. C., and Baek, K., "Inviscid Interactions Between Wake Vortices and Shear Layers," *Journal of Aircraft*, Vol. 36, No. 2, 1999, pp. 477–480.

[9]Mokry, M., "Hazard of Wake Vortex Encounters in Crosswind Shear," AIAA Paper 2003-0378, Jan. 2003.

Effect of Leading-Edge Cross-Sectional Shape on Nonslender Wing Rock

Lars E. Ericsson*
Mountain View, California 94040

Introduction

RECENT experimental results,[1] obtained in low-speed wind-tunnel tests, showed that the high-alpha rolling moment characteristics of a 45-deg delta wing are very sensitive to the cross-sectional shape of the leading edge, especially in regard to the unsteady aerodynamics. Figure 1 shows the geometric differences between the two tested delta wing models. The 9.1% thick wing had a semicircular leading-edge cross section, whereas the thin (1.25% thick) wing had a sharp-edged, 20-deg double bevel. As expected, the three-dimensional stall, realized when vortex breakdown reaches the apex,[2] occurs earliest on the sharp-edged delta wing (Fig. 2). For both wings, leading-edge flow separation with associated vortex shedding is delayed by an angle of attack $\Delta\alpha_v$, where $\Delta\alpha_v$ is determined by the leading-edge cross section as follows[3]:

$$\Delta\alpha_v = \tan^{-1}(\tan\alpha_{\mathrm{LE}}\cos\Lambda) \tag{1}$$

where α_{LE} is the crossflow angle of attack (normal to the leading edge) that has to be exceeded before crossflow separation occurs and a leading-edge vortex starts being generated. For the sharp-edged wing, $\alpha_{\mathrm{LE}} = 10$ deg. For the thick wing, α_{LE} is determined by the nose roundness[4] (Fig. 3). According to the experimental airfoil results in Fig. 3, one expects that $\alpha_{\mathrm{LE}} \geq 16$ deg for the thick wing. With $\Lambda = 45$ deg, these values of α_{LE} give, in Eq. (1), $\alpha_v = 7.1$ and $\alpha_v \geq 11.4$ deg for the thin and thick wing, respectively. The $\Delta\alpha_v \geq 4.3$ deg difference is in basic agreement with the experimental results in Fig. 2, showing maximum lift to occur at $\alpha \approx 20$ and 25 deg, respectively, for the thin and thick wing. This implies that the breakdown progresses with increasing $\alpha_{\mathrm{eff}} = \alpha - \alpha_v$ at roughly the same rate in the two cases.

Received 4 April 2001; revision received 10 October 2002; accepted for publication 17 October 2002. Copyright © 2003 by Lars E. Ericsson. Published by the American Institute of Aeronautics and Astronautics, Inc., with permission. Copies of this paper may be made for personal or internal use, on condition that the copier pay the $10.00 per-copy fee to the Copyright Clearance Center, Inc., 222 Rosewood Drive, Danvers, MA 01923; include the code 0021-8669/03 $10.00 in correspondence with the CCC.

*Engineering Consultant. Fellow AIAA.

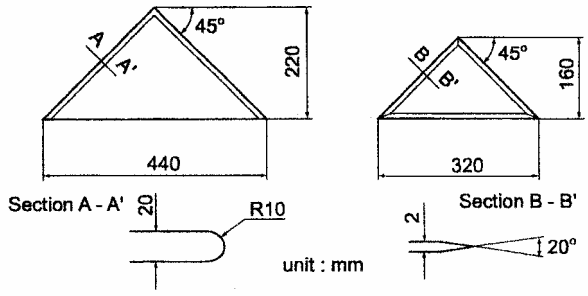

Fig. 1 Tested nonslender delta-wing models.[1]

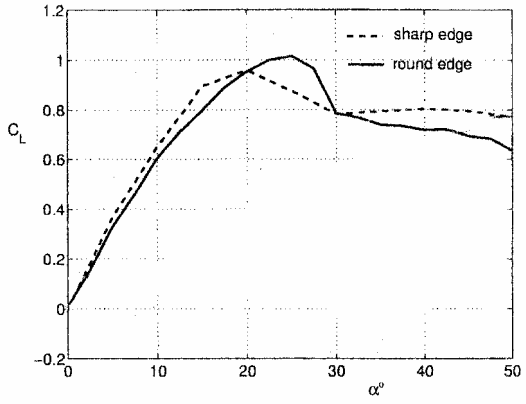

Fig. 2 Effect of leading-edge cross-sectional shape on lift characteristics $C_L(\alpha)$ of 45-deg delta wing.[1]

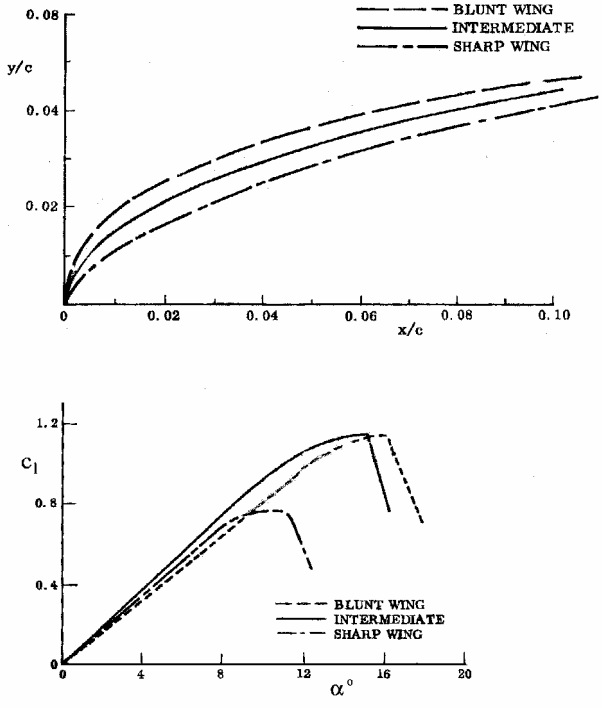

Fig. 3 Effect of leading-edge cross-sectional shape on airfoil lift characteristics $c_l(\alpha)$ (Ref. 4).

Roll-Trim Characteristics

Figure 4a shows the rolling moment characteristics $C_\ell(\phi)$ for roll-axis inclinations $\sigma = 20, 25$, and 30 deg of the thin wing, and Fig. 4b shows $C_\ell(\phi)$ for roll-axis inclinations $\sigma = 25$, 30, and 35 deg of the thick wing. At $\sigma = 20$ deg, the thin wing has stable trim points at $\phi \approx 0$ and 40 deg (Fig. 4a). The corresponding results for the thick wing at $\sigma = 25$ deg show only one stable trim point, at $|\phi| \approx 50$ deg (Fig. 4b). When the roll axis is inclined to $\sigma = 25$ and 30 deg, the

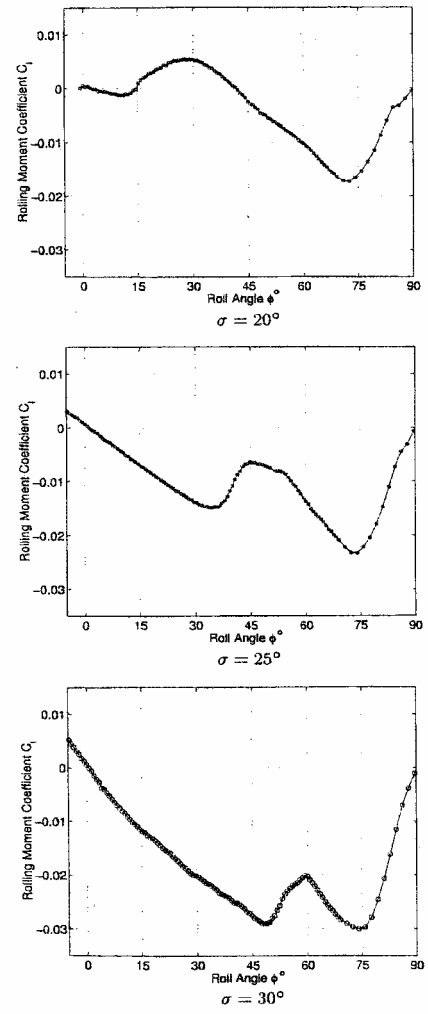

Fig. 4a Rolling moment characteristics of 45-deg delta wings[1] sharp leading edge.

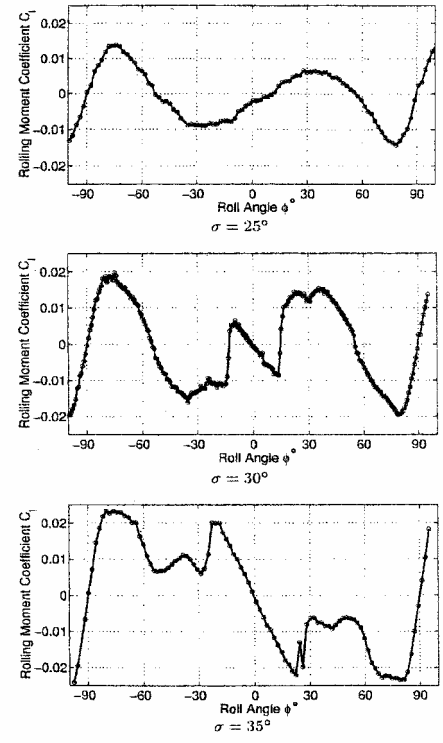

Fig. 4b Rolling moment characteristics of 45-deg delta wings[1] round leading edge.

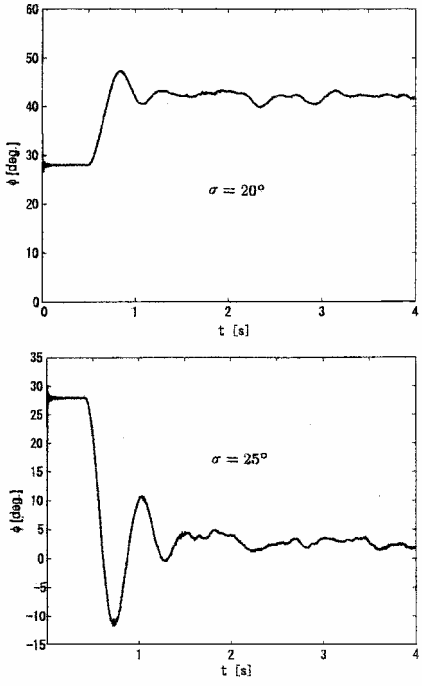

Fig. 5a Roll-angle time history of 45-deg delta wings[1] sharp leading edge.

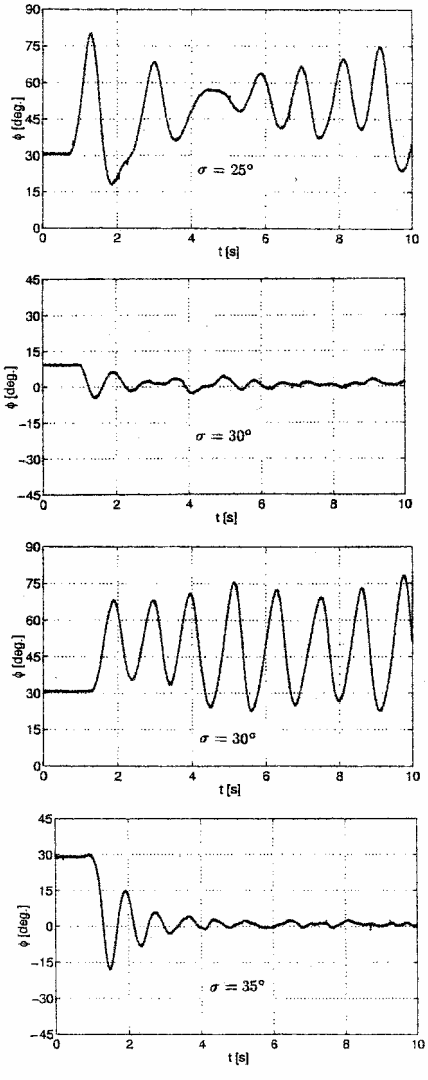

Fig. 5b Roll-angle time history of 45-deg delta wings[1] round leading edge.

thin wing has only the stable trim point at $\phi \approx 0$ (Fig. 4a). In contrast, Fig. 4b shows that at $\sigma = 30$ deg the thick wing adds a stable trim point at $\phi \approx 0$ to the one existing at $|\phi| \approx 50$ deg. At $\sigma = 35$ deg, the trim point at $|\phi| \approx 50$ deg is lost, leaving only the one at $\phi \approx 0$ for the range $-90 \leq \phi \leq 90$ deg, as was also the case for the thin wing at $\sigma = 25$ and 30 deg (Fig. 4a).

Roll-Oscillation Characteristics

The thin wing, released from $\phi \approx 28$ deg at $\sigma = 20$ deg, trims out at $\phi \approx 42$ deg (Fig. 5a), all in accordance with Fig. 4a. (If the release had been from $|\phi| < 10$ deg, the trim point would have been $\phi \approx 0$.) At $\sigma = 25$ deg, the release from $\phi \approx 28$ deg results in damped oscillations around the single, existing trim point at $\phi \approx 0$ (Fig. 5a). After the release of the thick wing from $\phi \approx 30$ deg at $\sigma = 25$ deg, the wing trims out at $\phi \approx 50$ deg (Fig. 5b), and the release from $\phi \approx 10$ and 30 deg at $\sigma = 30$ deg trims at $\phi \approx 0$ and 50 deg, respectively, all in accordance with the static trim characteristics (Fig. 4b). The release from $\phi = 30$ deg at $\sigma = 35$ deg trims out at the single, existing trim point at $\phi \approx 0$ (Fig. 5b).

Thus, the roll-trim characteristics are as expected for both wings. The difference between the two wings is the different character of the roll oscillations around the trim points. In the case of the thin wing (Fig. 5a), the roll oscillations are damped in all cases, whereas in the case of the thick wing only the oscillations around $\phi \approx 0$ (at $\sigma = 30$ and 35 deg) are damped (Fig. 5b). The oscillations around $\phi \approx 50$ deg at $\sigma = 25$ and 30 deg are undamped, resulting in limit-cycle oscillations of large amplitude.

In the case of the thin wing, the roll oscillations at $\sigma = 20$ deg around $\phi \approx 40$ deg and at $\sigma = 25$ deg around $\phi \approx 0$ (Fig. 5a) are highly damped. In the former case, $\sigma = 20$ deg and $\phi \approx 40$ deg, the effective leading-edge sweep and angle of attack can be determined as follows:

$$\Lambda(\phi) = \Lambda \pm \tan^{-1}(\tan\sigma \sin\phi) \tag{2}$$

$$\alpha(\phi) = \tan^{-1}(\tan\sigma \cos\phi) \tag{3}$$

Equations (2) and (3) give the following values for $\sigma = 20$ deg and $\phi \approx 40$ deg: $\Lambda(\phi) = 45 \pm 13.7$ deg, $\alpha(\phi) = 15.2$ deg. That is, the leeward wing-half has 58.7-deg effective leading-edge sweep and will produce roll damping at $\alpha(\phi) = 15.2$ deg according to earlier analysis.[5] The dipping, windward wing-half with its 31.3-deg leading-edge sweep will act as a straight wing with flat-plate cross section, contributing modestly to the roll damping according to the test results[6] in Fig. 6. The flow physics generating the limit-cycle-amplitude oscillations of the thick wing around $\phi \approx 50$ deg at $\sigma = 25$ and 30 deg were described in Ref. 7 from an analysis of the experimental results for a thick wing.[8] The damped roll oscillations around $\phi \approx 0$ of the thin wing at $\sigma = 25$ deg (Fig. 5a) and the thick wing at $\sigma = 30$ and 35 deg (Fig. 5b) are in agreement with expectations.[7,8]

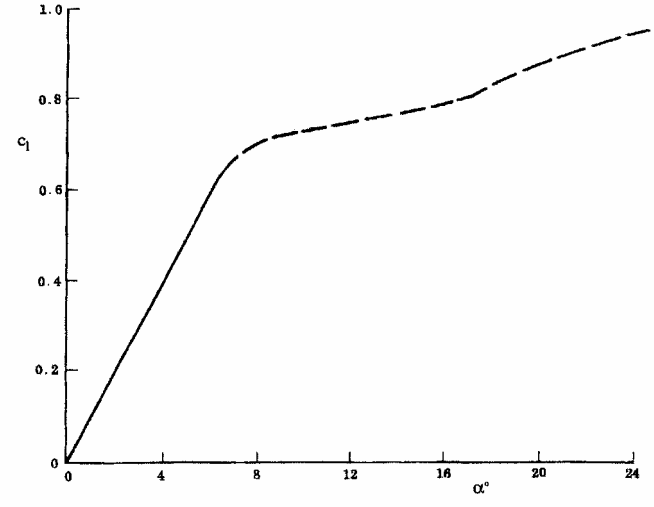

Fig. 6 Lift characteristics a flat-plate airfoil.[6]

Conclusions

An analysis of the high-alpha lateral stability of 45-deg delta wings reveals that nonslender wing rock can only occur on a wing with rounded leading edges that trims at a large roll angle. In that case, the dipping, windward wing-half will experience dynamic undamping of the type observed on stalling airfoils, driving the wing-rock motion. In contrast, when the leading edge is sharp, no wing rock occurs even at high angles of attack and roll because the leeward surface generates a dead-air-type of flow that has little effect on the roll damping and the attached flow on the windward side generates sufficient roll damping to prevent the wing rock from developing.

References

[1]Matsuno, T., and Nakamura, Y., "Self-Induced Roll Oscillation of 45-Degree Delta Wings," AIAA Paper 2000-0655, Jan. 2000.

[2]Bergmann, B., Hummel, D., and Oelker, H.-C., "Vortex Formation over a Close-Coupled Canard–Wing–Body Configuration in Unsymmetrical Flow," Paper 14, CP-494, AGARD, 1991.

[3]Ericsson, L. E., and King, H. H. C., "Effect of Leading-Edge Geometry on Delta Wing Unsteady Aerodynamics," *Journal of Aircraft*, Vol. 30, No. 5, 1993, pp. 793–795.

[4]Halfman, R. L., Johnson, H. C., and Haley, S. M., "Evaluation of High-Angle-of-Attack Aerodynamic Derivative Data and Stall Flutter Prediction Techniques," NACA TN 2533, 1951.

[5]Ericsson, L. E., and King, H. H. C., "Rapid Prediction of High-Alpha Unsteady Aerodynamics of Slender-Wing Aircraft," *Journal of Aircraft*, Vol. 29, No. 1, 1992, pp. 85–92.

[6]Critzos, C. C., Heyson, H. H., and Boswinkle, R. W., Jr., "Aerodynamic Characteristics of NACA-0012 Airfoil Section at Angles of Attack from 0 to 180°," NACA TN 3361, 1955.

[7]Ericsson, L. E., "Wing Rock of Non-Slender Delta Wings," *Journal of Aircraft*, Vol. 38, No. 1, 2001, pp. 36–41.

[8]Ueno, M., Matsuno, T., and Nakamura, Y., "Unsteady Aerodynamics of Rolling Thick Delta Wing with High Aspect Ratio," AIAA Paper 98-2520, Jan. 1998.

Calculating Flight Paths of Not Necessarily Small Inclination

John T. Lowry*
Flight Physics, San Marcos, Texas 78666

Introduction

ALTHOUGH the small flight-path angle approximation adequately treats routine operations of propeller/piston airplanes, its premise often fails to apply to modern jet aircraft with high thrust/weight ratios and might even be deficient for some maneuvers (e.g., steeply banked low-speed coordinated turns) of light airplanes. The historical reluctance[1] to move beyond the small path angle approximation was perhaps once understandable, but is no longer. This Note presents three graduated improvements (two analytical, one numerical) that can be used to solve a respectably comprehensive set (S-1) of aircraft center-of-mass equations of motion whenever better accuracy is needed. After describing those approximations and their solutions, sample calculations using each level of approximation are given for two jet aircraft climbing steeply at various bank angles. The author's future research plan is to use these enhanced flight-path approximations, together with improved modeling of the action of constant-speed propellers, to more realistically calculate tight or quick turn performance of Civil Air Patrol mountain search and rescue aircraft such as the Cessna 182 or 206.

Received 20 September 2002; revision received 4 November 2002; accepted for publication 5 November 2002. Copyright © 2002 by the American Institute of Aeronautics and Astronautics, Inc. All rights reserved. Copies of this paper may be made for personal or internal use, on condition that the copier pay the $10.00 per-copy fee to the Copyright Clearance Center, Inc., 222 Rosewood Drive, Danvers, MA 01923; include the code 0021-8669/03 $10.00 in correspondence with the CCC.

*Owner, 1615 Redwood Road, #12A. Member AIAA.

In cases of steady banked flight, aircraft trajectories are portions of helices. A given helical flight path can be described by radius R of the (right circular) cylinder on which it is wound, angular rotation rate ω, and steady rate of climb or descent $\dot{h}$. It turns out, however, that neither is R the flight-path radius of curvature ρ nor is ω the airplane's angular speed $\dot{\chi}$. Exact relations between those two pairs of variables will be derived next.

Four Graduated Sets of Equations for Steady Aircraft Motion

The base set of equations we are concerned with, S-1, is

$$T\cos(\alpha+\alpha_T) - D - W\sin\gamma = 0 \tag{1}$$

$$L\cos\varphi - W\cos\gamma + T\sin(\alpha+\alpha_T) = 0 \tag{2}$$

$$L\sin\varphi - Wv^2/g\rho = 0 \tag{3}$$

These equations come from considering forces 1) along the airplane's flight path, 2) perpendicular to the path and in the vertical direction, and 3) perpendicular to the path and in the horizontal direction. Those are directions of the common "trihedral" of right-handed orthonormal vectors $\hat{\boldsymbol{t}}, \hat{\boldsymbol{n}}, \hat{\boldsymbol{b}}$ of elementary differential geometry. Assuming the tie between lift L and angle of attack α given by a known relation $C_L(\alpha)$, Eqs. (1) and (2) are essentially in unknowns α (or lift L) and γ; Eq. (3) is in unknowns α (or L) and ρ.

Set S-1 incorporates assumptions that also apply (with further specific additions) to the three approximations to be considered: 1) no acceleration beyond the centripetal acceleration of a steady turn; 2) thrust offset α_T, if any, is constant and only in the airplane's plane of symmetry; 3) no side forces (only coordinated flight); 4) no "kinetic energy effect"; 5) aircraft weight W is constant during any single maneuver, as are thrust T, scalar airspeed v, and all of the rest of the featured variables; and 6) the drag polar is quadratic, $C_D = C_{D0} + KC_L^2$. The remainder of this section presents the four equation sets, in increasing order of exactitude, and remarks on their solutions. Frequent use will be made of standard variables and relations, such as

$$q \equiv \tfrac{1}{2}\rho v^2, \qquad L(\alpha) = qSC_L(\alpha)$$

$$D(\alpha) = D_P + D_i(\alpha) = qS\left[C_{D0} + KC_L^2(\alpha)\right] \tag{4}$$

often with additional subscripts to indicate the approximation being considered.

Small Flight-Path Angle γ_s (and Small Angles of Attack), S-4

This approximation is zeroth order in angles of attack—$\cos(\alpha+\alpha_T) \doteq 1$ and $\sin(\alpha+\alpha_T) \doteq 0$ and treats angle γ as small in the sense that $\cos\gamma \doteq 1$ but $\sin\gamma$ remains intact. The effect is to disentangle lift L from γ and immediately give one of the three needed solutions as

$$L_s = W/\cos\varphi \tag{5}$$

(Subscript s is for small flight-path angle.) Using the second of Eqs. (4), one gets

$$D_s = qSC_{D0} + \frac{KW^2}{qS\cos^2\varphi} = D_P + D_{\text{is}} \tag{6}$$

Because Eq. (1) is now approximated as

$$T - D_s - W\sin\gamma_s = 0 \tag{7}$$

we have a second and more important solution as

$$\sin\gamma_s = (T - D_s)/W \tag{8}$$

where it is understood that $(T - D_s) \ll W$. It is only left to solve Eq. (3), understanding a somewhat deficient $L \approx L_s$, to get (just as for level steady coordinated turns)

$$\rho_s = \frac{Wv^2}{gL_s\sin\varphi} = \frac{v^2}{g\tan\varphi} \tag{9}$$